Article

The Quantile-Matching Approach to Improving Radar Quantitative Precipitation Estimation in South China

Linye Song [1], Shangfeng Chen [2,*], Yun Li [3], Duo Qi [4], Jiankun Wu [1], Mingxuan Chen [1] and Weihua Cao [1]

1. Institute of Urban Meteorology, China Meteorological Administration, Beijing 100089, China; lysong@ium.cn (L.S.); jkwu@ium.cn (J.W.); mxchen@ium.cn (M.C.); whcao@ium.cn (W.C.)
2. Center for Monsoon System Research, Institute of Atmospheric Physics, Chinese Academy of Sciences, Beijing 100029, China
3. Business Intelligence and Data Analytics, Western Power, Perth, WA 6000, Australia; yun.li.wa@gmx.com
4. Heilongjiang Meteorological Observatory, Harbin 150001, China; qiduo@mail.iap.ac.cn
* Correspondence: chenshangfeng@mail.iap.ac.cn

Abstract: Weather radar provides regional rainfall information with a very high spatial and temporal resolution. Because the radar data suffer from errors from various sources, an accurate quantitative precipitation estimation (QPE) from a weather radar system is crucial for meteorological forecasts and hydrological applications. In the South China region, multiple weather radar networks are widely used, but the accuracy of radar QPE products remains to be analyzed and improved. Based on hourly radar QPE and rain gauge observation data, this study first analyzed the QPE error in South China and then applied the Quantile Matching (Q-matching) method to improve the radar QPE accuracy. The results show that the rainfall intensity of the radar QPE is generally larger than that determined from rain gauge observations but that it usually underestimates the intensity of the observed heavy rainfall. After the Q-matching method was applied to correct the QPE, the accuracy improved by a significant amount and was in good agreement with the rain gauge observations. Specifically, the Q-matching method was able to reduce the QPE error from 39–44%, demonstrating performance that is much better than that of the traditional climatological scaling method, which was shown to be able to reduce the QPE error from 3–15% in South China. Moreover, after the Q-matching correction, the QPE values were closer to the rainfall values that were observed from the automatic weather stations in terms of having a smaller mean absolute error and a higher correlation coefficient. Therefore, the Q-matching method can improve the QPE accuracy as well as estimate the surface precipitation better. This method provides a promising prospect for radar QPE in the study region.

Keywords: radar quantitative precipitation estimate; South China; quantile matching

1. Introduction

Precipitation is a key variable of weather forecasting and water cycle regulation, and it has pronounced impacts on both meteorological and hydrological processes. Extreme precipitation events can cause severe natural disasters, including flash floods, debris flow, and urban inland inundation [1–4], resulting in great economic losses and casualties to human society [5]. In recent decades, the Doppler weather radar has become an important method for precipitation monitoring [6–8] because accurate and timely areal rainfall data are crucial for hydrometeorological forecasting and early flash-flood warnings. Quantitative precipitation estimation (QPE) products can be generated by radar stereoscopic scanning observation by means of the transformational relationship between radar reflectivity (Z) and the surface rainfall rate (R). The radar QPE products are characterized by high spatial resolution and temporal continuity [9–12], which are crucial for hydrometeorological coupled forecasts and have already been wildly applied in many meteorological departments in China.

Surface precipitation is a complex weather phenomenon that demonstrates substantial spatial and temporal fluctuations and that is associated with a high degree of error and uncertainty. Radar is widely used in real time and has a high spatial resolution and temporal continuity; however, errors are always present in radar QPE products because it is an indirect rainfall measurement method. These errors can be caused by many factors, such as ground clutter, abnormal propagation, blockage by mountains and buildings, non-meteorological echoes, detection range, distance attenuation, bright band contamination, instrument calibration errors, changes in raindrop spectrum distribution, the empirical local Z–R relationship, and random errors [11,13–19]. On the other hand, conventional rain gauge measurements can provide direct and fairly accurate precipitation measurements at a single point [20]. Although rainfall observations at automatic weather stations (AWS) have certain limitations, including sparse station networks, especially in mountainous regions, and the possibility being unable to capture local small-scale convective storms [21,22], the rainfall intensity that is gauged at AWS is much more accurate than the rainfall intensity determined through indirect radar observations.

In the literature, various efforts have been made to improve the accuracy of high-precision rainfall from both radar and AWS rainfall data. To improve the accuracy of the radar QPE, instead of using the classic equation of $Z = 200R^{1.6}$ [23], studies have mainly focused on reconstructing the local Z–R relationship according to different climate regions, different seasons, and different rainfall types. This has demonstrated that the accuracy of radar QPE can be improved to some extent by applying a more appropriate local Z–R relationship [24–27]. In recent decades, many studies have also focused on merging AWS and radar rainfall data using various methods [22,28–32]. These methods were used to reduce precipitation estimation errors and include bias correction [33–35], the Kalman filter [36–38], optimum interpolation [39,40], the variation method [41–44], kriging, cokriging, kriging with external drift [45–47], conditional merging [48], frequency matching [49], and the multi-step combination of different methods based on average weight, the optimal integration of artificial intelligence, and the statistical weight matrix [50–52]. Recently, Song et al. [53] proposed a climatological correction algorithm to improve the accuracy of the rainfall amount estimations from the Beijing Auto NowCasting (BJ-ANC) system [24] using a long time series of radar QPE and AWS precipitation data for the North China region. However, whether the scaling method can be adequately applied for other systems or other regions is still unknown. Therefore, it is necessary to investigate the applicability and possible limitation of the climatological scaling method for improving QPE accuracy in the South China region.

Similar to the climatological scaling method, the Quantile Matching (Q-matching) method [54–56] is also an approach that is generally used in climate change studies. Previous studies have demonstrated that the Q-matching method can be employed to correct the outputs of general climate models (GCM) with respect to observations, and it has served as a statistical downscaling method in other climate sciences [56,57]. The Q-matching method has been applied outside of China for precipitation correction. For example, previous studies have found that quantile mapping showed the best performance, especially at high quantiles, compared to seven other methods that were implemented to reduce the regional climate model error over the Alpine region [58]. Chen et al. [59] compared six bias correction methods including two quantile methods that were based on an empirical distribution and a gamma distribution to conduct bias correction for hydrological modeling over ten North American river basins. The quantile mapping bias correction method was proposed to correct radar data that were located at the Hannover airport in Germany [34]. It has also been applied for satellite precipitation products in the Guiana Shield [35]. Nonetheless, it is unknown whether the Q-matching method can be used for the application of reducing QPE errors on an hourly timescale in China, particularly for the South China region.

In this study, we will demonstrate that the climatological scaling method is not subject to different systems or regions. Furthermore, based on comparison analysis, it is also indicated that the Q-matching method can also be applied for reducing radar QPE error

and that it is able to show a much better performance than the climatological scaling method that is commonly used for the South China region. It should be noted that other spatially integrative methods are worth comparing, but that is out of the scope of this study.

The remainder of the paper is arranged as follows: Section 2 describes the data and methods in detail. Results are given in Section 3. In particular, the errors of the original QPE are calculated in Section 3.1. Additionally, Section 3.2 compares the correction results between the Q-matching and the climatological scaling correction methods, including verification by means of large samples and a case study. Finally, the conclusion and discussion are given in Sections 4 and 5, respectively.

2. Data and Methods

The study area (21.0–26.0°N, 108–118°E) in this research is located in the South China region and includes the Guangdong Province and parts of the Guangxi, Hunan, Jiangxi, Fujian, and Guizhou Provinces. It covers a drainage area of approximately 6.15×10^5 km^2. There are 6083 automatic meteorological stations in the South China region (Figure 1). This area is relatively flat and has a station altitude that is generally less than 600 m. However, the topography is relatively complex and is characterized by mountainous and hilly areas. Low topography is mostly found along the coastline and in the Pearl River Delta region (Figure 1), which is one of the most economically developed regions in China. The area is mainly influenced by East Asian summer monsoons and South China Sea summer monsoons and receives the bulk of its annual precipitation in the summer season [60–62].

Two precipitation datasets are employed in this study and include rain gauge observations from AWS and QPE that were obtained from the Severe Weather Auto Nowcasting (hereinafter referred to as SWAN) System [63]. The range for single radar is 230 km, and the range gate differs from different radars. There are 17 radars in the study region of South China (Figure 1). Mixed scans from layers 1–3 were used, and the beam width was not controlled. The radar data were quality control checked in order to determine the ground clutter and electromagnetic interference [64]. A 6 min time interval was used for the volume scans. Observational rainfall measurement from the AWS network were interpolated to a 1 km $\times$ 1 km resolution via an inverse distance-weighted method that corresponded to that of the spatial resolution of the radar QPE from the SWAN system. The maximum radius and maximum adjacent station number parameters that were used interpolation were 100 km and 8 stations, respectively. It is necessary to acknowledge that the inverse distance squared usually tends to generate precipitation bullseyes, especially when the interpolation at each grid point is taken for all of the stations. Hence, a limitation of a 100 km radius and a fixed number of the nearest 8 stations were chosen for this study in order to alleviate this undesirable tendency and to make the interpolation method more similar to if a human conducted the analysis by hand. For example, only the nearest eight stations are taken into account when interpolation is conducted through Integrated Nowcasting when using the Comprehensive Analysis system [65]. It should be noted that the results in the present study are generally the same as to if other parameters, such as if a 150 km radius or 10 stations were used (Figures not shown). In addition, the gridded radar QPE dataset with a 1 km$\times$ 1 km resolution is interpolated to station locations through a bilinear interpolation method, which is used to calculate the QPE error when compared to the AWS observations. This study collected data for the summers of 2019–2020 (June–July–August) from both the AWS and QPE datasets, where the time resolution was set to 1 h. It should be noted that invalid samples were not employed in the present study. An invalid sample was determined either the AWS or the radar QPE had missing data for a specific hour. In other words, only valid data samples that were available from both datasets were selected and calculated. Therefore, 3732 h valid time samples were defined in total. August 2019 had the highest number of valid samples, and July 2020 had the highest number of invalid samples(Figure 2). For the total 3732 valid sample hours and 6083 station sites (t = 3721, s = 6083), there were a total of 2,347,413 samples after the data that did not include informa-

tion regarding rainfall from the AWS observations were removed (i.e., remaining $AWS_{t,s}$ samples ≥ 0.1 mm/h).
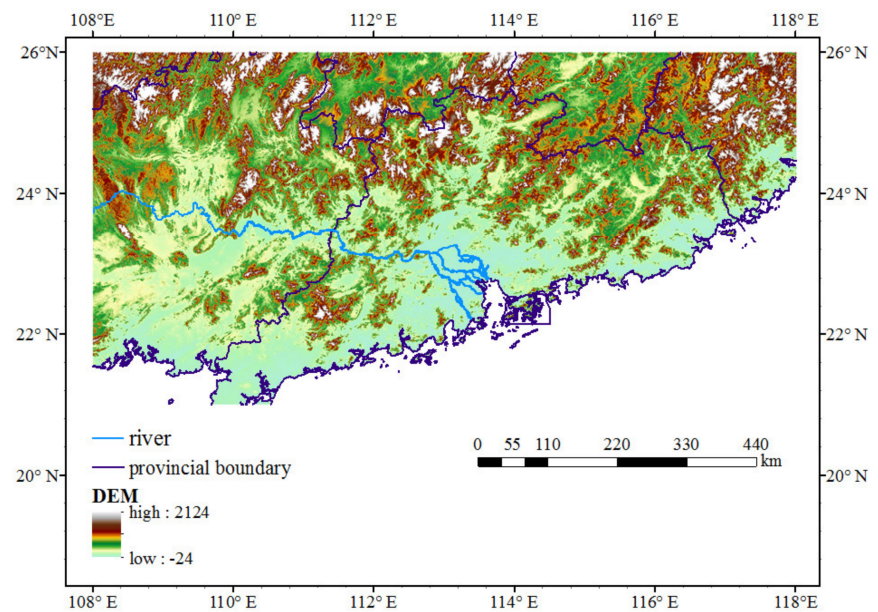
(a)
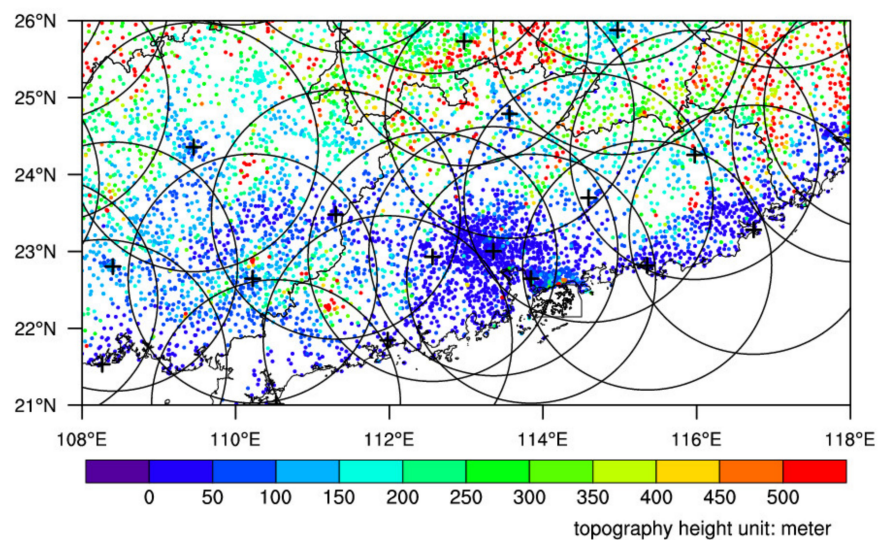
(b)

Figure 1. (**a**) The topography distribution in the study area of South China. (**b**) Schematic diagram of station distribution (indicated by dots) and radar locations (denoted by + and circles) in the South China region. The colors at each dot represent the topography height (unit: meter) at the corresponding station points. The 17 radars include Guangzhou (SA), Heyuan (SA), Meizhou (SA), Shantou (SA), Shanwei (SA), Shaoguan (SA), Shenzhen (SA), Yangjiang (SA), Zhanjiang (SA), Zhaoqing (SA), Liuzhou (SB), Nanning (SA), Wuzhou (SB), Fangchenggang (SA), Yulin (SA), Chenzhou (SA), and Ganzhou (SC).

This study uses two methods to improve the radar QPE in the South China region. One method is the climatological scaling correction algorithm [53]. It is suggested that the error of radar QPE can be reduced after applying the climatological correction scaling algorithm. In particular, the high-resolution rainfall structure can be well-captured, and the

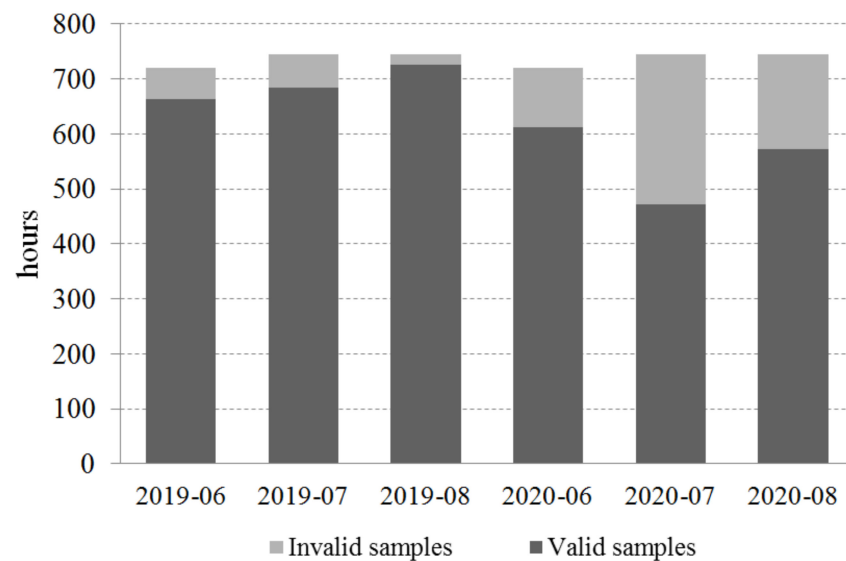strength of the QPE rainfall is closer to that of the AWS observations for the North China region [53].

Figure 2. The number (unit: hours) of valid samples and invalid samples in the summer (June, July, and August) during 2019–2020. Valid samples are defined as data that are present in both the AWS and radar QPE data for each hour. Otherwise, the sample was determined to be invalid otherwise and could not be used in the analysis.

The climatological correction scaling algorithm [53] is introduced simply and appears as follows: First, the station calibration coefficient C_s was calculated. Second, the c gridded calibration coefficient $C_g(i,j)$ was calculated. Then, the final climatic scaling factor was obtained and used to calculate the corrected radar QPE according to Equation (3).

$$C_s = \frac{\sum_{t=1}^{T} R_{s,t}}{\sum_{t=1}^{T} Q_{s,t}} \tag{1}$$

$$C_g(i,j) = \frac{\sum_{t=1}^{T} R(i,j,t)}{\sum_{t=1}^{T} Q(i,j,t)} \tag{2}$$

$$Q_1^*(i,j,t) = \max[C_s, C_g(i,j)] \times Q(i,j,t) \tag{3}$$

where $R_{s,t}$ is the AWS rainfall at station s, and t is the time period in hourly intervals, starting from $t = 1$, which represents the first hourly rainfall period, and increasing throughout the entire study period (i.e., $t = T = 3732$ h for JJA in the 2019–2020 period); $Q_{s,t}$ is the corresponding QPE value at station s and t; $R(i,j,t)$ and $Q(i,j,t)$ are the interpreted AWS rainfall and QPE value at a radar cell grid (i,j) and at a specific time t; $Q_1^*(i,j,t)$ is the corrected QPE value $Q(i,j,t)$ and can be obtained by applying the climatological correction scaling algorithm (1)–(3).

Another method that was employed in this study is the Q-matching method. As described in several studies, the basic premise of this method is to correct one data source by considering another data source to be correct by comparing their probability distribution functions. This process contains two steps: (i) the probability distributions are first fitted to hourly rainfall from the AWS stations and the corresponding QPE data; (ii) the quantile of the QPE value is estimated (the data source to be corrected) from its cumulative distribution

function (CDF) by considering the estimated quantile and using the inverse of the CDF of the observed station data [34]. If we assume that the AWS network is capable of providing correct information and if the rainfall distribution as determined from the AWS data is same as the one obtained from the QPE data, then the correction procedure for the QPE data based on the Q-matching method can be formulated by

$$Q_2^*(i,j,t) = F_{AWS,t}^{-1}(F_{rad,t}(Q(i,j,t)))$$
(4)

where $Q_2^*(i,j,t)$ is the corrected value of the original QPE $Q(i,j,t)$ at the cell grid (i,j) and time t, $F_{rad,t}$ is the CDF estimated from the radar data $Q(i,j,t)$ at time t, and $F_{AWS,t}^{-1}$ is the inverse CDF $F_{AWS,t}$ from the AWS rain gauge network at time t, which converts the quantiles that were estimated by $F_{rad,t}$ back to the corrected QPE value $Q_2^*(i,j,t)$. The estimates of $F_{AWS,t}$, $F_{rad,t}$ and $F_{AWS,t}^{-1}$ are $\hat{F}_{AWS,t}$, $\hat{F}_{rad,t}$ and $\hat{F}_{AWS,t}^{-1}$, respectively, and were empirically and modally from the historical AWS observation and QPE data [66].

The QPE accuracy is evaluated using the quantitative statistical parameters of the mean absolute error (MAE), root-mean-square error (RMSE), and correlation coefficient (CC). They are given as follows:

$$MAE = \frac{1}{n}\sum_{i=1}^{n}|Y_i - O_i|$$
(5)

$$RMSE = \sqrt{\frac{1}{n}\sum_{i=1}^{n}(Y_i - O_i)^2}$$
(6)

$$CC = \frac{\sum\limits_{i=1}^{n}(Y_i - \overline{Y})(O_i - \overline{O})}{\sqrt{\sum\limits_{i=1}^{n}(Y_i - \overline{Y})^2 \cdot \sum\limits_{i=1}^{n}(O_i - \overline{O})^2}}$$
(7)

where n is the sample number, i is a given station, Y_i and $\overline{Y}$ is a generic notation for QPE and the mean of the original QPE products from the SWAN system or from the QPE after correction. O_i and $\overline{O}$ are the observational AWS rainfall and mean.

In addition, the QPE accuracy is also validated based on the Nash–Sutcliffe Efficiency (*NSE*) and the Kling–Gupta Efficiency (*KGE*), both of which are often used as traditional metrics in hydrology [67,68]. They are calculated through the following equations:

$$NSE = 1 - \frac{\sum\limits_{i=1}^{n}(Y_i - O_i)^2}{\sum\limits_{i=1}^{n}(O_i - \overline{O})^2}$$
(8)

$$KGE = 1 - \sqrt{(CC - 1)^2 + (\frac{\sigma_Y}{\sigma_X} - 1)^2 + (\frac{\mu_Y}{\mu_X} - 1)^2}$$
(9)

where CC is the linear correlation coefficient in Equation (7). σ_X and σ_Y are the standard deviations in the AWS observations and in the QPE estimations, respectively. μ_X and μ_Y are the means (i.e., equivalent to $\overline{O}$ and $\overline{Y}$, respectively). *NSE* = 1 indicates perfect agreement between the simulations and the observations. *NSE* < 0 indicates that the model is a worse predictor than the mean of observations. Similar to the *NSE*, a *KGE* = 1 also indicates perfect correspondence. Higher efficiency values represent observations that are closer to being able to be reproduced perfectly.

In terms of the categorical metrics, the two skills scores of probability of detection (POD) and the false alarm ratio (FAR) were also employed. Here, multiple thresholds corresponding to different precipitation levels were evaluated. To calculate the scores at a specific threshold P (P = 1 mm/h, 5 mm/h, 10 mm/h, 15 mm/h, and 20 mm/h), the values

in the QPE estimation and the true AWS vales are first converted to 0/1 by thresholding them with P, and a(truth = 1, estimation = 1), b(truth = 0, estimation = 1), c(truth = 1, estimation = 0), and d(truth = 0, estimation = 0) are then calculated. The POD and FAR scores are calculated as follows:

$$POD = \frac{a}{a + c} \tag{10}$$

$$FAR = \frac{b}{a + b} \tag{11}$$

3. Results

3.1. QPE Errors

Figure 3 shows the box plot for the hourly rainfall as determined by the AWS rainy observations and the corresponding radar estimations. The median value was 0.6 mm/h for all of the AWS samples, while the median radar QPE value was 0.9 mm/h, indicating that the rainfall amount that was estimated from the radar QPE was generally larger than that of the AWS rainfall amount (Figure 3a). For the 75% quartile value, the rainfall amount that was estimated from the radar QPE was also larger than the AWS rainfall amount. However, the 25% quartile value of the radar QPE was closer to zero, which is smaller than that of the AWS rainfall value (Figure 3a). In addition, a phenomenon was observed wherein the radar was unable to capture any incidence of precipitation at a specific location, even when this location was found to be rainy through AWS observations. These characteristics tended to be contributed rainfall samples that were falling at a rate of less than 20 mm/h (Figure 3b). For heavy rainfall samples with an hourly amount that was larger than 20 mm/h, however, the characteristics were reversed. It was found that the radar QPE often underestimates the precipitation amount for heavy rainfall events, with the median value being shown to be smaller than that of the AWS observations (Figure 3c). It is also true for the 25% and 75% quartile values, which show that the radar QPE often underestimates rainfall amount.
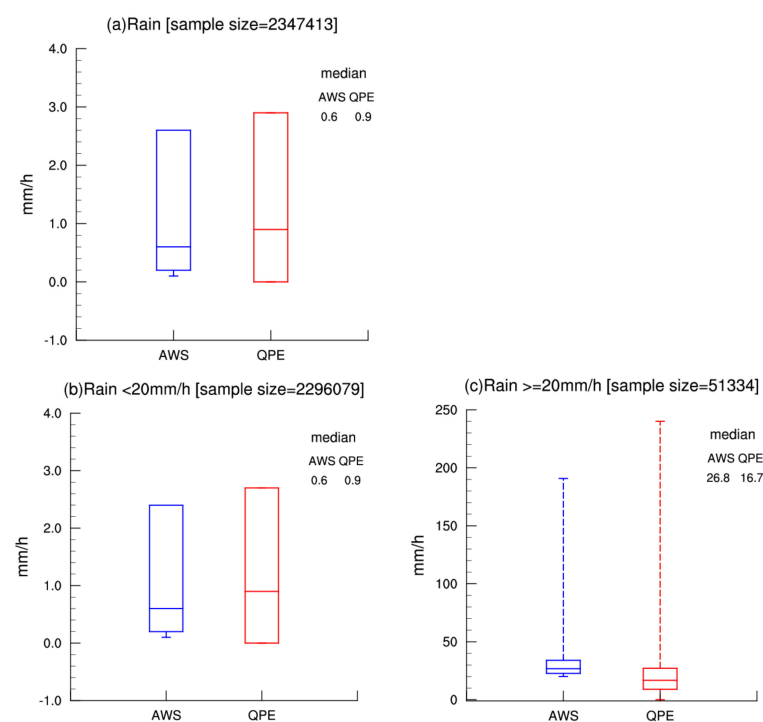

Figure 3. The box plot of the hourly rain for the AWS and radar QPE (unit: mm/h) based on (**a**) all samples, (**b**) samples of rainfall less than 20 mm/h, and (**c**) samples of rainfall larger than (including equal to) 20 mm/h. In each box, the top (bottom) of the box indicates the 75% (25%) quartile, and the middle of the box provides the median value. In (**c**), the maximum and minimum are shown with the highest and lowest bar.

Figure 4 compares the spatial distribution of the total rainfall amount in the summer by comparing the values from the interpolated AWS observation and the QPE products that were obtained from the SWAN system. Large differences are shown to occur most parts of the South China region. On the coast of South China, specifically in the Pearl River Delta region, the accumulated rainfall values that were determined by means of radar QPE are larger than the AWS values (Figure 4a,b). However, the QPE values are mainly smaller than the AWS observations in the interior region of western and northern South China. The spatial distribution of the QPE and AWS rainfall difference was also calculated. Obvious overestimation exists in large areas of the coast of South China, and this difference can reach up to 1500 mm in parts of the Pearl River Delta and Zhanjiang regions (Figure 4c). The largest underestimation exists in the western central South China region, where the difference value is about −1000 mm. The remaining regions are generally characterized with a small difference that is closer to zero (Figure 4c).
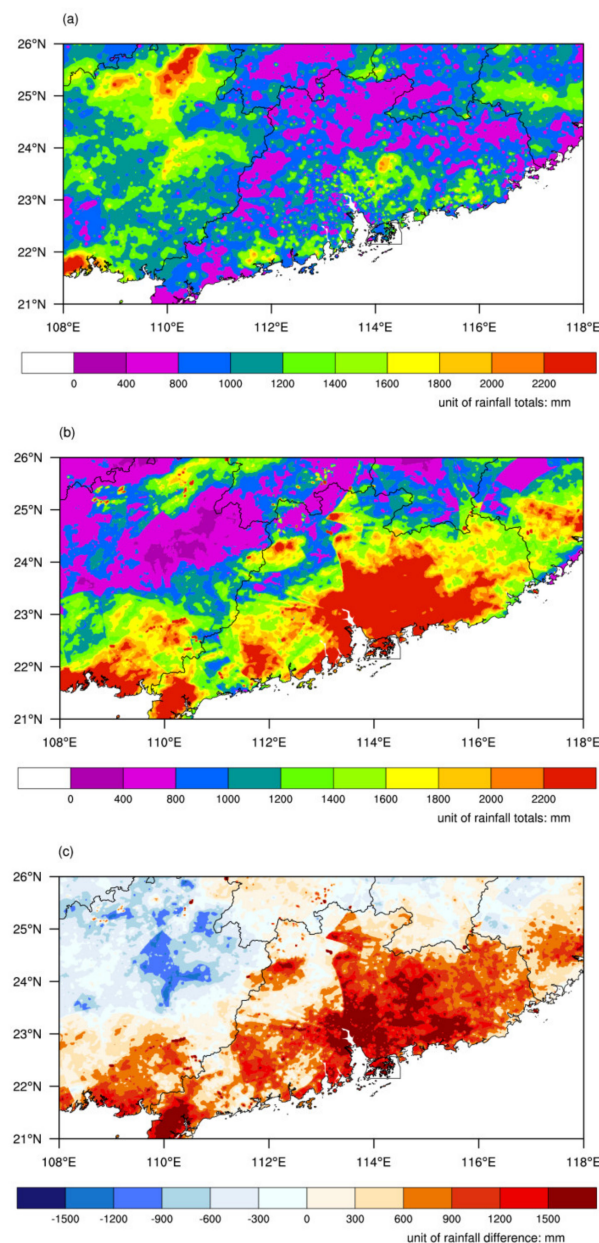

Figure 4. Distribution of summer rainfall totals (unit: mm) for the years 2019–2020. (**a**) Interpolated AWS rainfall totals, (**b**) radar QPE rainfall totals, (**c**) and difference between radar QPE and AWS rainfall.

The results of the error and correlation coefficient are given in Table 1. The values demonstrate that the averaged MAE and RMSE of the QPE products that were obtained from the SWAN system in the South China region is 2.237 mm/h and 4.948 mm/h, respectively. The average CC is 0.629, with a standard deviation of 0.16 among all the station locations, which mostly ranges from 0.56 to 0.75 between the 25% and 75% quartiles. Gao et al. [40] showed that the RMSE of the QPE from the Z–R relationship is approximately 4.52–5.98 mm/h based on six individual radars located in Guangzhou, Meizhou, Shaoguan, Shantou, Yangjiang and Shenzhen.

Table 1. The results of MAE, RMSE error, and CC of hourly radar QPE products compared to AWS rain observations. The results and improvement percentages are also given after the scaling and Q-matching methods were implemented, respectively. The units for MAE and RMSE are mm/h.

	Original QPE	QPE after Scaling	QPE after Q-Matching	Improvement by Scaling	Improvement by Q-Matching
MAE	2.237	1.947	1.257	12.96%	43.81%
RMSE	4.948	4.323	3.011	14.46%	39.15%
CC	0.629	0.650	0.893	3.34%	41.97%

3.2. Comparison of the Climatological Correction Scaling Algorithm and Q-matching Methods

Figure 5 displays the result of the climatic scaling factor field in the South China region that was obtained based on the climatological scaling correction algorithm that was described in Section 2. It should be noted that an empirical maximum of the scaling factor parameter was set as 2.0 in this study in order to avoid excessive correction. This is because in some mountainous regions where the radar beam is shielded by mountains, the radar detecting signal may be very weak or even nonexistent, thus leading to very low and unreasonable precipitation estimations [53,65]. In those regions, the climatological scaling correction algorithm may yield an arbitrarily high scaling factor and may eventually yield corrected questionable precipitation values. It should be noted that the obtained results are generally similar if the maximum scaling factor is set as 2.5 or 3.0 in order to avoid an undesirable effect. Figure 5 clearly shows that the scaling factors are less than one in almost all of the regions that comprise the South China coast, indicating that the radar QPE is usually stronger than the AWS rainfall observations that were determined on a long-term time scale (Figure 5). In contrast, the scaling factors are greater than one in the majority of the regions belonging to north-western South China and some parts of north-eastern South China, demonstrating that radar QPE is often weaker than the rainfall amount that is determined by AWS (Figure 5). The closer the scaling factor is to one, the more accurate the radar rainfall estimation is when determined on a long-term time scale. The distribution of the scaling factor field may be related to the topography of the South China region to some extent (Figures 1 and 5).

The probability density functions (PDF) of the precipitation difference between the original QPE and AWS for small-to-moderate hourly rainfall samples of less than 20 mm/h are shown in Figure 6a. Normal distribution is seen from the difference between QPE and AWS, demonstrating that the radar estimation error is in a relatively ideal state. It should be noted that the PDF distribution of all of the hourly rainfall samples, regardless of rainfall intensity, is generally similar to what is seen in Figure 6a. However, when we focus on heavy rainfall samples that are larger than or equal to 20 mm/h, then it is obvious that the PDF distribution is not normally distributed (Figure 6b). The peak occurs at the difference of about −15 mm/h, demonstrating negative skewness and indicating that the QPE tends to underestimate large amounts of rainfall, which is in agreement with the results shown in Figure 3c. This non-Gaussian characteristic can still be seen in the PDF distribution of the QPE error after correction by the scaling method even though the precipitation difference distribution becomes more concentrated than that of the original QPE products (Figure 6d). However, the QPE error is much closer to that of a Gaussian distribution

after correction by means of the Q-matching method, both for light and heavy rainfall (Figure 6e,f). In particular, the distorted probability distribution has been significantly revised for hourly rainfall amounts that are larger than 20 mm/h, with the peak being located at the difference value, which is close to 0 (Figure 6f). Therefore, the above results indicate that after applying the Q-matching method, the probability density functions of the corrected QPE are closer than the AWS observations, while the climatological scaling method cannot achieve this correction effect.
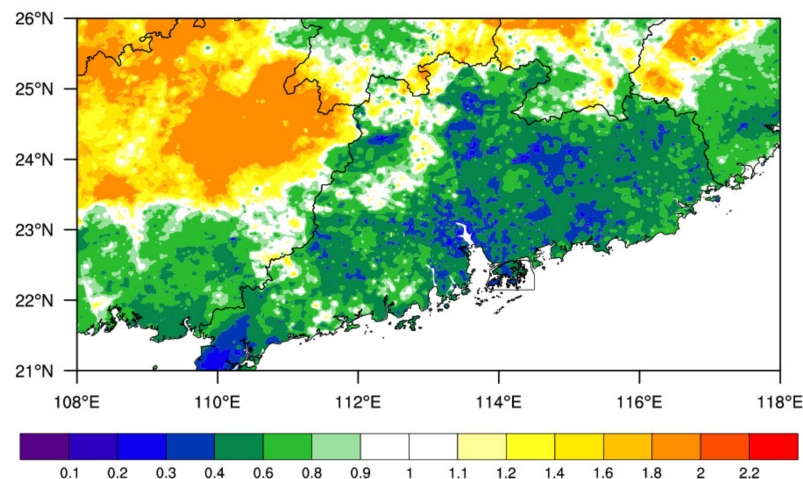

Figure 5. The results o F field correction calculated by means of the climatological scaling method.

To further compare the rainfall accuracy distribution between the scaling and Q-matching methods, the spatial fields of the correction coefficients between the QPE after correction and the AWS observational rainfall are shown in Figure 7. After scaling correction, a large correction coefficient can be seen in most parts of South China, except for the northern part of Guangdong province (Figure 7a). The original QPE also demonstrates is lowest accuracy in this region (figure not shown). The average correction coefficient for all of the stations increased from 0.63 to 0.650, and the averaged MAE error is shown to be reduced from 2.24 to 1.95 (Table 1). These indicate that the QPE accuracy is slightly superior after climatological scaling correction. Furthermore, the correlation coefficients between QPE and AWS rainfall increase above 0.9 in most parts of South China after Q-matching correction (Figure 7b). It should be noted that there are 200 stations with a correlation coefficient less than 0.9, with most ranging from about 0.4 to 0.9. The lowest correlation coefficients mainly occur in the north-central part of South China (Figure 7b), and only a few occur along the coastal areas. However, compared to the application of the scaling method, the Q-matching method performed much better across the entire region (Figure 7a,b). The average correction coefficient for all of the stations increased from 0.63 to 0.89, and the averaged MAE error reduced from 2.24 to 1.26 (Table 1). In a word, the QPE error in South China reduced from 3–15% as measured by different statistics after the scaling method was applied (Table 1). However, the QPE error reduced a significant amount, from 39–44%, after the Q-matching method was applied (Table 1), which performed much better than the scaling algorithm did. In addition, the categorical metrics of POD and FAR were also compared. After applying the climatological scaling method, the POD is decreased compared to the original QPE products, while the FAR is reduced for all thresholds. This demonstrates that the climatological scaling method results in worse detection probability (Table 2); although FAR score demonstrates an improvement of 18–20% (Table 3). This means that the climatological scaling correction tends to generate an excessive transformation that introduces negative bias. However, an increased POD score and a decreased FAR score were obtained for the 1 mm/h, 5 mm/h, 10 mm/h, 15 mm/h, and 20 mm/h thresholds, representing all of the categories, after the Q-matching correction method was applied, with an improvement percentage of 20–81% and 34–45% being measured by POD

and FAR, respectively. This indicates that the Q-matching method is able to achieve a better performance than the scaling method (Tables 2 and 3). Furthermore, the *NSE* increased from 0.209 to 0.396 after correction by means of the climatological scaling method, while increases that were much higher to 0.707 were achieved after correction by means of the Q-matching method. As for the *KGE*, it the value decreased from 0.620 to 0.532 after the climatological scaling correction was applied, indicating bad performance in terms of the *KGE* metric. However, the *KGE* increased to 0.741 after the Q-matching correction was applied, which is closer to 1. These results demonstrate that the Q-matching algorithm is better able to improve the radar QPE accuracy over the South China region than the climatological scaling algorithm.
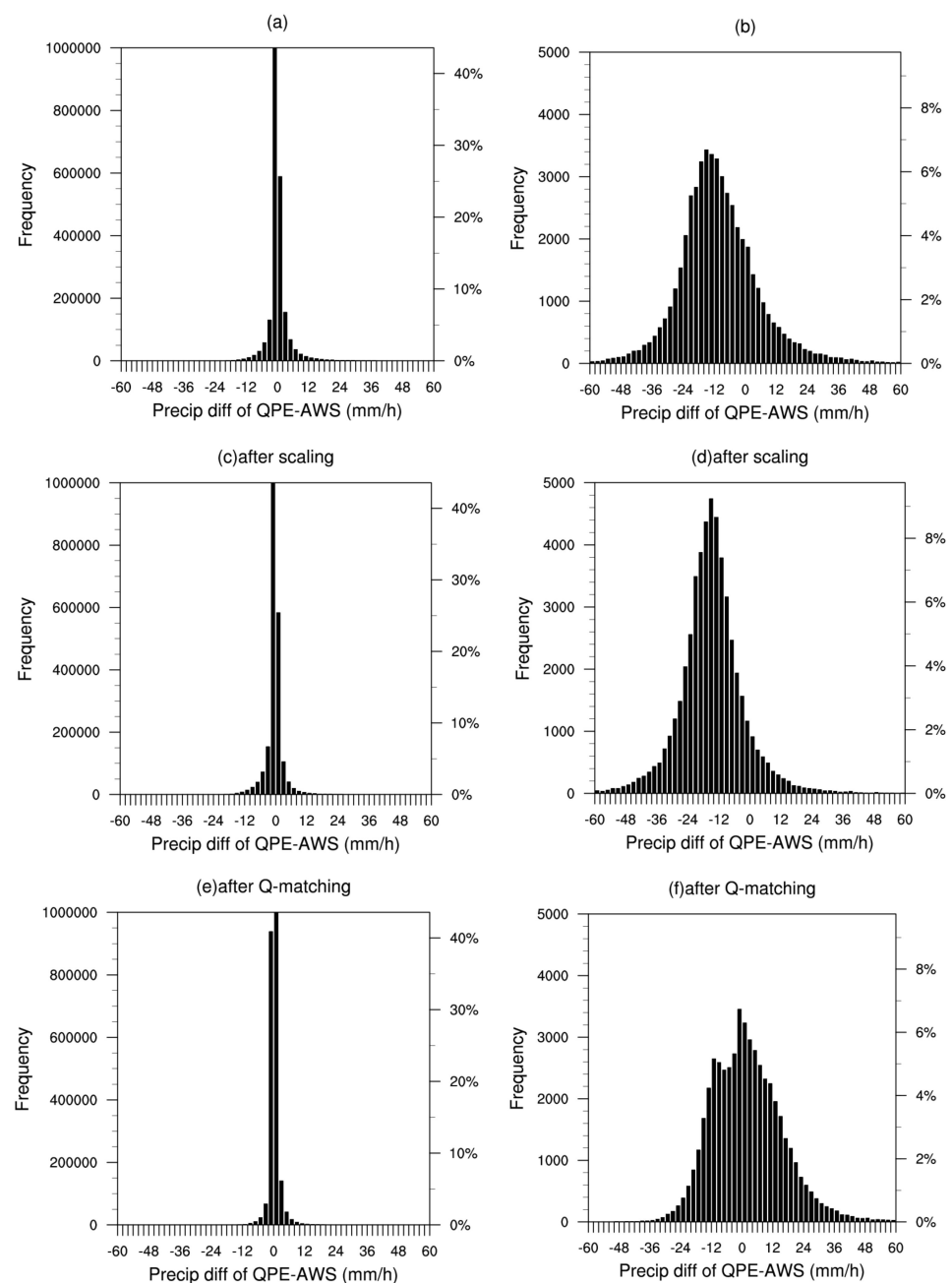
Figure 6. The probability density function of the precipitation difference between QPE and AWS for (**a**,**b**) original radar QPE product, (**c**,**d**) after correction by scaling, (**e**,**f**) and after correction by Q-matching. (**a**,**c**,**e**) are for hourly rainfall samples less than 20 mm/h, and (**b**,**d**,**f**) are for heavy rainfall that are larger than and equal to 20 mm/h.

A precipitation case on 20 August 2020, 07am UTC is displayed in Figure 8. In this case, the strongest precipitation center is located in the southeastern region of South China, and the maximum rainfall intensity is more than 40 mm/h (Figure 8a). Compared to the AWS observations, the estimated precipitation center of the radar QPE is slightly weaker (Figure 8b). The corrected QPE that have been interpolated to the different station locations are shown in Figure 8c,d after the scaling and Q-matching methods had been applied. After applying the Q-matching method, the QPE rainfall intensity was closer to that of the AWS observations (Figure 8a,d), with the exception some sites in the Pearl River Delta region. In this case, the maximum precipitation center is even weaker after the scaling correction (Figure 8c), which can mainly be attributed to the fact that the scaling factor is constantly less than one, as the radar overestimates rainfall in this area from the perspective of a long-term statistical result (Figure 5). However, for the whole of the South China region, the scaling method still shows an improvement, with the correlation coefficient between QPE and AWS rainfall increasing from 0.68 to 0.78 (Figure 9a,c). The scatter plot that was obtained after the Q-matching correction is much closer to the diagonal line, and the correlation coefficient between the QPE and AWS rainfall values increased from 0.68 to 0.90 (Figure 9b). The above results demonstrate that the climatological scaling method can be applied for the South China region, while the Q-matching method performs better than the scaling algorithm and shows a promising prospect for application in improving the accuracy of radar QPE.
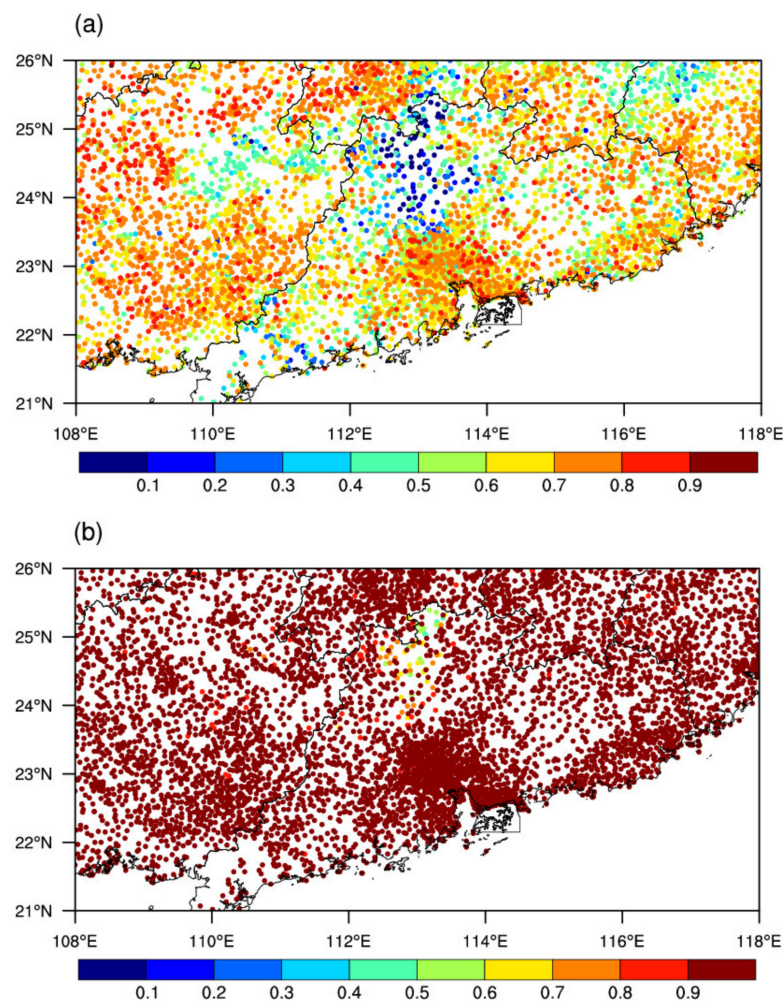

Figure 7. The spatial distribution of the correlation coefficients between the radar QPE product and AWS observational station rainfall (**a**) after correction by scaling and (**b**) after correction by Q-matching, respectively.

Table 2. The results of POD scores for 1 mm/h, 5 mm/h, 10 mm/h, 15 mm/h, and 20 mm/h thresholds of hourly radar QPE products compared to AWS rain observations. The improvement percentages are also given after correction methods by means of scaling and Q-matching.

	1 mm/h	5 mm/h	10 mm/h	15 mm/h	20 mm/h
original QPE	0.756	0.609	0.523	0.460	0.411
QPE after scaling	0.702	0.512	0.393	0.314	0.257
QPE after Q-matching	0.914	0.840	0.786	0.756	0.741
Improvement by scaling	−7.14%	−15.93%	−24.86%	−31.74%	−37.47%
Improvement by Q-matching	20.90%	37.93%	50.29%	64.35%	80.29%

Table 3. Same as Table 2 but for the results of the FAR scores.

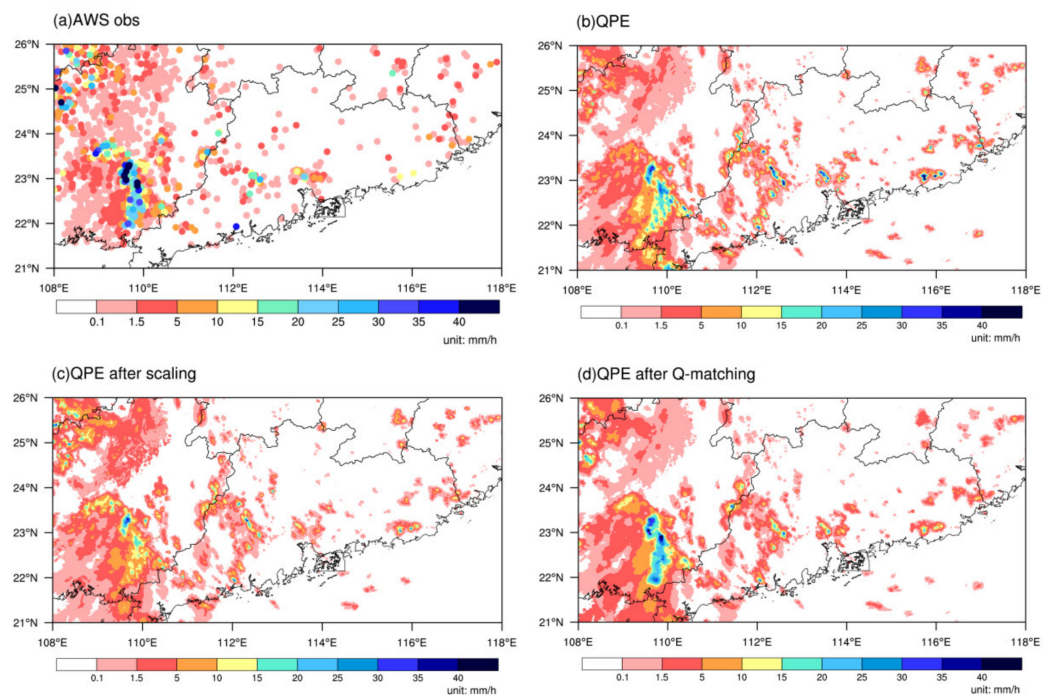|	1 mm/h	5 mm/h	10 mm/h	15 mm/h	20 mm/h
original QPE	0.323	0.438	0.497	0.559	0.612
QPE after scaling	0.262	0.354	0.398	0.448	0.495
QPE after Q-matching	0.188	0.241	0.280	0.337	0.398
Improvement by scaling	18.89%	19.18%	19.92%	19.86%	19.12%
Improvement by Q-matching	41.80%	44.98%	43.66%	39.71%	34.97%

Figure 8. Precipitation case study on 07 UTC 20 August 2020. (**a**) AWS observational rainfall. (**b**) The original radar QPE products. (**c**) QPE after correction by scaling. (**d**) QPE after correction by Q-matching. Unit is mm/h.
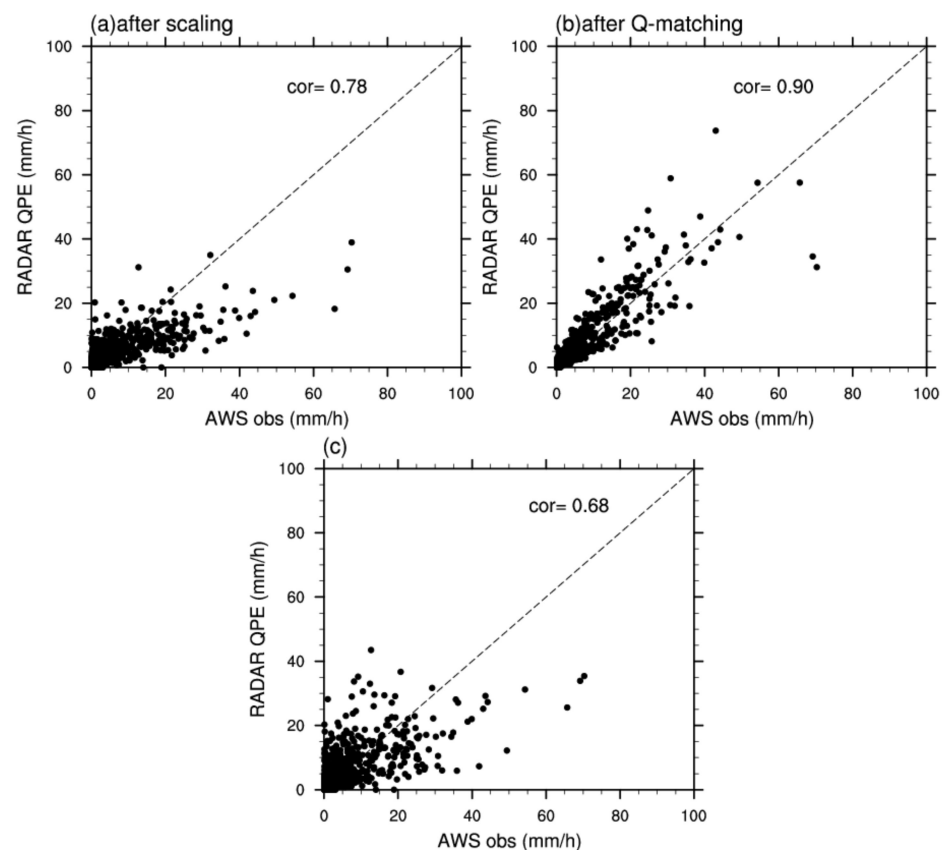
Figure 9. Scatter plot of hourly rainfall on 07 UTC 20 August 2020 between AWS and radar QPE (**a**) after correction by scaling, (**b**) after correction by Q-matching, and (**c**) before correction. The horizontal axis represents AWS rainfall, and the vertical axis represents radar QPE. The correlation coefficient is also shown.

4. Conclusions

This study evaluates the errors of 1 radar QPE precipitation products that have been accumulated hourly from the SWAN system in the South China region and further proposes a new Q-matching method to improve the radar quantitative precipitation estimations. The climatological scaling method, which was previously used for the North China region, is also applied to correct the QPE to examine whether it is appropriate for use in the South China region. Furthermore, these two methods were compared with each other to determine the performance of the correction effects. The main conclusions are stated below:

Although the QPE accuracy based on the Z–R relationship ranged from reasonable levels, there is a lot of room for improvement. The averaged QPE product errors that were obtained in the South China region were 2.237 mm/h and 4.948 mm/h, as measured by MAE and RMSE, respectively. In terms of intensity, the rainfall amount that was determined by radar QPE was generally larger than the AWS rainfall amount. However, for heavy rainfall samples with hourly amounts that were larger than 20 mm/h, it was found that the QPE generally underestimates the rainfall amount. In addition, a phenomenon was observed where in the radar was not able to capture the precipitation at the specific area, even when the AWS indicated that the area was rainy. From the view of spatial distribution, the results show that the accumulated QPE are larger than those of the AWS rainfall values found on the South China coast, especially in the Pearl River Delta region. In contrast, the accumulated QPE rainfall was generally weaker than the AWS observations in the interior region of western and northern South China. The region with the poorest QPE accuracy was found to be located at the northern part of Guangdong province.

The results demonstrate that the climatological scaling and Q-matching methods can both achieve positive effects in correcting the accuracy of radar rainfall estimations for the

South China region. As indicated by Song et al. [53], the climatological scaling algorithm is easy to transplant into different regions or different systems. After scaling correction, the QPE error in South China was reduced from 3–15%, as measured by different statistics in terms of MAE, RMSE, and CC. However, after Q-matching correction, the QPE error was largely reduced from 39–44%, demonstrating a much better performance. As for POD, FAR, *NSE*, and KEG metrics, the Q-matching method was also shown to perform better than the scaling method in the South China region. The QPE is in good agreement with rain gauge observations after correction by the Q-matching method. The good performance of the Q-matching method may mainly be because it fully considers the distributions of two different data sources (AWS and QPE); that is, the Q-matching method assumes that the rainfall distribution from the AWS network is the same as the one of the QPE data that were obtained from the weather radar. The QPE accuracy improved dramatically after Q-matching correction, as demonstrated by the fact that the correlation coefficient between the radar QPE and AWS rainfall amount significantly increased all over South China. The probability density function distribution of the hourly QPE is much closer to the observations, both for light small and heavy rainfall. As a whole, this study indicates that the Q-matching method can be used to further improve the accuracy of radar QPE compared to the original QPE products and QPE after scaling correction.

5. Discussion

From the above results, we demonstrated that in South China, the Q-matching method is better than the climatological scaling method for correcting radar QPE. However, there are still some issues that remain unresolved. For example, whether the Q-matching method could be applied to improve the QPE and whether it would perform better than the scaling method in northern China is still worth further analysis. In addition, whether the Q-matching method that was proposed in the present study could be applied to other areas around the world remains to be investigated. In the majority of the South China region, the correlation coefficient reached values of above 0.6. However, the poorest QPE accuracy is found to be located in the north-central part of South China and in the northern part of Guangdong province in particular, where the lowest correlation coefficient was determined between the QPE and AWS rainfall, showing values that were below 0.3; additionally, improvement was shown to be limited, regardless of which correction method was applied. The reasons why the north central South China region shows the poorest accuracy in terms of both the original QPE products and the corrected QPE than other regions and what may cause this uncertainty still need to be investigated further. Furthermore, in this study, we only compared two methods: climatological scaling and the Q-matching; other spatially integrative methods are also worth further exploration in the near future.

Author Contributions: Conceptualization, S.C. and L.S.; methodology, L.S., Y.L. and S.C.; software, S.C., L.S. and Y.L.; validation, L.S., S.C., D.Q. and Y.L.; formal analysis, L.S. and S.C.; investigation, L.S. and S.C.; resources, L.S., Y.L. and S.C.; data curation, L.S., S.C., Y.L., D.Q., J.W., M.C. and W.C.; writing—original draft preparation, L.S., S.C., and Y.L.; writing—review and editing, L.S. and S.C.; visualization, L.S. and S.C.; supervision, L.S. and S.C. All authors have read and agreed to the published version of the manuscript.

References

1. Pellarin, T.G.; Delrieu, G.M.; Saulnier, H.A. Hydrologic visibility of weather radars operating in mountainous regions: Case study for the Ardeche catchment (France). *J. Hydrometeorol.* **2002**, *3*, 539–555. [CrossRef]
2. Maggioni, V.; Massari, C. On the performance of satellite precipitation products in riverine flood modeling: A review. *J. Hydrol.* **2018**, *558*, 214–224. [CrossRef]
3. Yin, Z.C.; Guo, W.L.; Li, N.J.; Xie, Y.Y. Numerical simulation of urban ponding in Beijing. *Meteorol. Mon.* **2012**, *41*, 1111–1118. (In Chinese)
4. Zhao, W.; Chen, S.; Chen, W.; Yao, S.; Nath, D.; Yu, B. Interannual variations of the rainy season withdrawal of the monsoon transitional zone in China. *Clim. Dyn.* **2019**, *53*, 2031–2046. [CrossRef]
5. Jonkman, S.N. Global Perspectives on Loss of Human Life Caused by Floods. *Nat. Hazards* **2005**, *34*, 151–175. [CrossRef]
6. Yu, X.D. Detection and Warnings of Severe Convection with Doppler Weather Radar. *Adv. Meteorol. Sci. Technol.* **2011**, *1*, 31–41. (In Chinese)
7. Wang, Y.; Han, L.; Wang, H.Q. Statistical characteristics of convective initiation in the Beijing-Tianjin region revealed by six-year radar data. *J. Meteorol. Res.* **2014**, *28*, 1127–1136. [CrossRef]
8. Gabella, M.; Speirs, P.; Hamann, U.; Germann, U.; Berne, A. Measurement of Precipitation in the Alps Using Dual-Polarization C-Band Ground-Based Radars, the GPM Spaceborne Ku-Band Radar, and Rain Gauges. *Remote Sens.* **2017**, *9*, 1147. [CrossRef]
9. Germann, U.; Galli, G.; Boscacci, M.; Bolliger, M. Radar precipitation measurement in a mountainous region. *Q. J. R. Meteorol. Soc.* **2006**, *132*, 1669–1692. [CrossRef]
10. Berne, A.; Krajewski, W.F. Radar for hydrology: Unfulfilled promise or unrecognized potential? *Adv. Water Resour.* **2013**, *51*, 357–366. [CrossRef]
11. Zhuang, W. Key Method Research on Radar Precipitation Estimation of Complex Terrain over the Tibet Plateau. Ph.D. Thesis, Chinese Academy of Meteorological Sciences, Beijing, China, 2013; p. 128. (In Chinese)
12. Wang, H.Y.; Wang, G.L.; Liu, L.P.; Jiang, Y.; Wang, D.; Feng, L.I. Development of a-real time quality control method for automatic rainfall gauge data using radar quantitative precipitation estimation. *Chin. J. Atmos. Sci.* **2015**, *39*, 59–67. (In Chinese)
13. Steiner, M.; Smith, J.A. Use of Three-Dimensional reflectivity structure for automated detection and removal of nonpre-cipitating echoes in radar data. *J. Atmos. Ocean. Technol.* **2002**, *19*, 673–686. [CrossRef]
14. Gabella, M. Improving Operational Measurement of Precipitation Using Radar in Mountainous Terrain—Part II: Verification and Applications. *IEEE Geosci. Remote Sens. Lett.* **2004**, *1*, 84–89. [CrossRef]
15. Parker, M.D.; Knievel, J.C. Do Meteorologists Suppress Thunderstorms?: Radar-Derived Statistics and the Behavior of Moist Convection. *Bull. Am. Meteorol. Soc.* **2005**, *86*, 341–358. [CrossRef]
16. Prat, O.P.; Barros, A.P. Exploring the transient behavior of Z-R relationships: Implications for radar rainfall estimation. *Am. Meteorol. Soc.* **2009**, *48*, 2127–2143. [CrossRef]
17. Krajewski, W.F.; Villarini, G.; Smith, J.A. Radar-Rainfall Uncertainties: Where are we after thirty years of effort? *Bull. Am. Meteorol. Soc.* **2010**, *91*, 87–94. [CrossRef]
18. Ku, J.M.; Ro, Y.; Kim, K.; Yoo, C. Analysis on Characteristics of Orographic Effect about the Rainfall Using Radar Data: A Case Study on Chungju Dam Basin. *J. Korea Water Resour. Assoc.* **2015**, *48*, 393–407. [CrossRef]
19. Jacobi, S.; Heistermann, M. Benchmarking attenuation correction procedures for six years of single-polarized C-band weather radar observations in South-West Germany. *Geomat. Nat. Hazards Risk* **2016**, *7*, 1785–1799. [CrossRef]
20. Cong, F.; Liu, L. A comprehensive analysis of data from the CINRAD and the ground rainfall station. *Meteorol. Monogr.* **2011**, *37*, 532–539.
21. Lee, J.; Byun, H.; Kim, H.; Jun, H. Evaluation of a rain gauge network considering the spatial distribution characteristics and entropy: A case study of Imha dam basin. *J. Korean Soc. Hazard. Mitig.* **2013**, *13*, 217–226. [CrossRef]
22. Ochoa-Rodriguez, S.; Wang, L.-P.; Willems, P.; Onof, C. A Review of Radar-Rain Gauge Data Merging Methods and Their Potential for Urban Hydrological Applications. *Water Resour. Res.* **2019**, *55*, 6356–6391. [CrossRef]
23. Marshall, J.S.; Palmer, W.M.K. The distribution of raindrops with size. *J. Meteorol.* **1948**, *5*, 165–166. [CrossRef]
24. Chen, M.X.; Gao, F.; Kong, R.; Wang, Y.; Ding, Q. Introduction of auto-nowcasting system for convective storm and its performance in Beijing Olympics meteorological service. *J. Appl. Meteorol. Sci.* **2010**, *21*, 395–404. (In Chinese)

25. Wang, G.L.; Liu, L.P.; Ding, Y.Y. Improvement of radar quantitative precipitation estimation based on real-time adjustments to Z-R relationships and inverse distance weighting correction schemes. *Adv. Atmos. Sci.* **2012**, *29*, 575–584. [CrossRef]
26. Gou, Y.B.; Liu, L.; Wang, D.; Zhong, L.; Chen, C. Evaluation and analysis of the Z-R storm-grouping relationships fitting scheme based on storm identification. *Torrential Rain Disasters* **2015**, *34*, 1–8.
27. Zhang, J.; Howard, K.W.; Langston, C.; Kaney, B.; Qi, Y.; Tang, L.; Grams, H.; Wang, Y.; Cocks, S.; Martinaitis, S.M.; et al. Multi-Radar Multi-Sensor (MRMS) Quantitative Precipitation Estimation: Initial Operating Capabilities. *Bull. Am. Meteorol. Soc.* **2016**, *97*, 621–638. [CrossRef]
28. Goudenhoofdt, E.; Delobbe, L. Evaluation of radar-gauge merging methods for quantitative precipitation estimates. *Hydrol. Earth Syst. Sci.* **2009**, *13*, 195–203. [CrossRef]
29. Wang, L.P.; Ochoa-Rodriguez, S.; Simões, N.; Onof, C.; Maksimovic, Č. Radar-rain gauge data combination techniques: A revision and analysis of their suitability for urban hydrology. *Water Sci. Technol.* **2013**, *68*, 737–747. [CrossRef]
30. Li, J.T.; Li, B.; Yang, H.P.; Liu, X.Y.; Zhang, L.; Guo, L. A study of regional rainfall estimation by using radar and rain gauge: Proposal of model integration method. *Meteorol. Sci. Technol.* **2014**, *42*, 556–562.
31. Berndt, C.; Rabiei, E.; Haberlandt, U. Geostatistical merging of rain gauge and radar data for high temporal resolutions and various station density scenarios. *J. Hydrol.* **2014**, *508*, 88–101. [CrossRef]
32. Hasan, M.M.; Sharma, A.; Mariethoz, G.; Johnson, F.; Seed, A. Improving radar rainfall estimation by merging point rainfall measurements within a model combination framework. *Adv. Water Resour.* **2016**, *97*, 205–218. [CrossRef]
33. Seo, D.J.; Breidenbach, J.P.; Johnson, E.R. Real-time estimation of mean field bias in radar rainfall data. *J. Hydrol.* **1999**, *223*, 131–147. [CrossRef]
34. Rabiei, E.; Haberlandt, U. Applying bias correction for merging rain gauge and radar data. *J. Hydrol.* **2015**, *522*, 544–557. [CrossRef]
35. Ringard, J.; Seyler, F.; Linguet, L. A Quantile Mapping Bias Correction Method Based on Hydroclimatic Classification of the Guiana Shield. *Sensors* **2017**, *17*, 1413. [CrossRef] [PubMed]
36. Chumchean, S.; Seed, A.; Sharma, A. Correcting of real-time radar rainfall bias using a Kalman filtering approach. *J. Hydrol.* **2006**, *317*, 123–137. [CrossRef]
37. Kim, J.; Yoo, C. Using Extended Kalman Filter for Real-time Decision of Parameters of Z-R Relationship. *J. Korea Water Resour. Assoc.* **2014**, *47*, 119–133. [CrossRef]
38. Kim, J.; Yoo, C. Use of a dual Kalman filter for real-time correction of mean field bias of radar rain rate. *J. Hydrol.* **2014**, *519*, 2785–2796. [CrossRef]
39. Álvarez, V.H.; Aznar, M. An efficient approach to optimal interpolation of experimental data. *J. Taiwan Inst. Chem. Eng.* **2010**, *41*, 184–189. [CrossRef]
40. Gao, X.R.; Liang, J.Y.; Li, C.H. Radar quantitative precipitation estimation techniques and effect evaluation. *J. Trop. Meteorol.* **2012**, *28*, 77–88. (In Chinese)
41. Fu, D.S.; Dai, T.P. Application of the variational method in the calibration of regional rainfall measurement by weather radar. *J. Nanjing Inst. Meteorol.* **1990**, *13*, 598–603. (In Chinese)
42. Zhang, P.C.; Dai, T.P.; Fu, D.S.; Wu, Z.F. Principle and accuracy of adjusting the area precipitation from digital weather radar through variational method. *Chin. J. Atmos. Sci.* **1992**, *16*, 248–256.
43. Deng, X.J.; Huang, H.H.; Wu, D. Application of variational method for the calibration radar quantitative estimates of precip-itation. *Q. J. Appl. Meteorol.* **2000**, *11*, 255–256. (In Chinese)
44. Bianchi, B.; van Leeuwen, P.J.; Hogan, R.; Berne, A. A Variational Approach to Retrieve Rain Rate by Combining Information from Rain Gauges, Radars, and Microwave Links. *J. Hydrometeorol.* **2013**, *14*, 1897–1909. [CrossRef]
45. Krajewski, W.F. Cokriging radar-rainfall and rain gage data. *J. Geophys. Res. Space Phys.* **1987**, *92*, 9571–9580. [CrossRef]
46. Sideris, I.V.; Gabella, M.; Erdin, R.; Germann, U. Real-time radar–rain gauge merging using spatio-temporal co-kriging with external drift in the alpine terrain of Switzerland. *Q. J. R. Meteorol. Soc.* **2014**, *140*, 1097–1111. [CrossRef]
47. Cantet, P. Mapping the mean monthly precipitation of a small island using kriging with external drifts. *Theor. Appl. Clim.* **2015**, *127*, 31–44. [CrossRef]
48. Sinclair, S.; Pegram, G. Combining radar and rain gauge rainfall estimates using conditional merging. *Atmos. Sci. Lett.* **2005**, *6*, 19–22. [CrossRef]
49. Zhu, Y.; Luo, Y. Precipitation Calibration Based on the Frequency-Matching Method. *Weather. Forecast.* **2015**, *30*, 1109–1124. [CrossRef]
50. Wu, M.C.; Lin, G.F.; Hwang, L.R.; Chen, D.Y.C.; Chiang, C.C.; Wang, Y.C. Optimal Integration of the Ensemble Forecasts from an Ensemble Quantitative Precipitation Forecast Experiment. *Procedia Eng.* **2016**, *154*, 1291–1297. [CrossRef]
51. Chao, L.; Zhang, K.; Li, Z.; Zhu, Y.; Wang, J.; Yu, Z. Geographically weighted regression based methods for merging satellite and gauge precipitation. *J. Hydrol.* **2018**, *558*, 275–289. [CrossRef]
52. Shao, Y.; Fu, A.; Zhao, J.; Xu, J.; Wu, J. Improving quantitative precipitation estimates by radar-rain gauge merging and an inte-gration algorithm in the Yishu River catchment, China. *Theor. Appl. Climatol.* **2021**, *144*, 611–623. [CrossRef]
53. Song, L.Y.; Chen, M.X.; Cheng, C.L.; Gao, F.; Chen, M. Characteristics of summer QPE error and a climatological correction method over Beijing-Tianjin-Hebei region. *Acta Meteorol. Sin.* **2019**, *77*, 497–515. (In Chinese)

54. Panofsky, H.A.; Brier, G.W. *Some Applications of Statistics to Meteorology*; Penn State University Press: University Park, PA, USA, 1958; p. 234.
55. Haddad, Z.S.; Rosenfeld, D. Optimality of empirical Z-R relations. *Meteorol. Soc.* **1997**, *123*, 1283–1293. [CrossRef]
56. Maraun, D. Bias Correction, Quantile Mapping, and Downscaling: Revisiting the Inflation Issue. *J. Clim.* **2013**, *26*, 2137–2143. [CrossRef]
57. Vrac, M.; Ayar, P.V. Influence of Bias Correcting Predictors on Statistical Downscaling Models. *J. Appl. Meteorol. Clim.* **2017**, *56*, 5–26. [CrossRef]
58. Matthias, J.; Themeßl, M.; Gobiet, A.; Leuprecht, A. Empirical–statistical downscaling and error correction of daily precip-itation from regional climate models. *Int. J. Climatol.* **2010**, *31*, 1530–1544.
59. Chen, J.; Brissette, F.P.; Chaumont, D.; Braun, M. Finding appropriate bias correction methods in downscaling precipitation for hydrologic impact studies over North America. *Water Resour. Res.* **2013**, *49*, 4187–4205. [CrossRef]
60. Song, L.Y.; Duan, W.S.; Li, Y.; Mao, J.Y. A timescale decomposed threshold regression downscaling approach to forecasting South China early summer rainfall. *Adv. Atmos. Sci.* **2016**, *33*, 1071–1084. [CrossRef]
61. Hu, P.; Chen, W.; Chen, S.; Huang, R. Interannual variability and triggers of the South China Sea summer monsoon withdrawal. *Clim. Dyn.* **2019**, *53*, 4355–4372. [CrossRef]
62. Hu, P.; Chen, W.; Chen, S.; Liu, Y.; Huang, R. Extremely Early Summer Monsoon Onset in the South China Sea in 2019 Following an El Niño Event. *Mon. Weather. Rev.* **2020**, *148*, 1877–1890. [CrossRef]
63. Han, F.; Wo, W.F. Design and Implementation of SWAN2.0 Platform. *J. Appl. Meteorol. Sci.* **2018**, *29*, 25–34. (In Chinese)
64. Wen, H.; Liu, L.P.; Zhang, C.A.; Yin, C.; Zhang, Y.; Cheng, S. Operational evaluation of radar data quality control for ground clutter and electromagnetic interference. *J. Meteorol. Sci.* **2016**, *36*, 789–799.
65. Haiden, T.; Kann, A.; Pistotnik, G.; Stadlbacher, K.; Wittmann, C. Integrated Nowcasting through Comprehensive Analysis (INCA)—System description. *ZAMG Rep.* **2010**, 59. Available online: http://www.zamg.ac.at/fix/INCA_system.pdf (accessed on 20 June 2021).
66. Michelangeli, P.-A.; Vrac, M.; Loukos, H. Probabilistic Downscaling Approaches: Application to Wind Cumulative Dis-tribution Functions. *Geophys. Res. Lett.* **2009**, *36*. [CrossRef]
67. Nash, J.E.; Sutcliffe, J.V. River flow forecasting through conceptual models part I—A discussion of principles. *J. Hydrol.* **1970**, *10*, 282–290. [CrossRef]
68. Knoben, W.J.M.; Freer, J.E.; Woods, R.A. Inherent benchmark or not? Comparing Nash–Sutcliffe and Kling–Gupta efficiency scores. *Hydrol. Earth Syst. Sci.* **2019**, *23*, 4323–4331. [CrossRef]